Electrical and structural properties of low resistivity tin-doped indium oxide films

Yuzo Shigesato,[a] Satoru Takaki, and Takeshi Haranoh
Advanced Glass R&D Center, Asahi Glass Co., Ltd. 1150, Hazawa-cho, Kanagawa-ku, Yokohama-shi, Kanagawa 221, Japan

(Received 1 November 1991; accepted for publication 2 January 1992)

Tin-doped indium oxide (ITO) films with the resistivity less than 1.35×10^{-4} Ω cm were formed by low voltage dc magnetron sputtering (LVMS) and highly dense plasma-assisted electron beam (EB) evaporation using the arc plasma generator (HDPE). The structural properties of these films were investigated using x-ray diffraction, scanning electron microscope, and electron spectroscopy for chemical analysis, in comparison with the films formed by conventional magnetron sputtering and EB evaporation, in order to clarify the key factors for low resistivity. With decreasing plasma impedance and sputtering voltages from 540 to 380 V, the resistivity of the films deposited at $T_s = 400$ °C decreased from 1.92 to 1.34×10^{-4} Ω cm, due mostly to increase in the carrier density. This LVMS film showed higher crystallinity because of lower damages of high-energy particles during the deposition, which might increase the number of electrically active species. For HDPE, the film with resistance of 1.23×10^{-4} Ω cm was deposited at $T_s = 280$ °C, which showed more flat surface morphology and less surface segregation of tin than the conventional EB films.

I. INTRODUCTION

Tin-doped indium oxide (ITO) films are highly degenerated wide gap semiconductors with the high conductivity and high transparency in the visible region of the spectrum. They are widely used in information displays, such as LCDs, ELDs, or ECDs. With recent demands for larger size and high quality display panels, ITO films are required to have lower resistivity of less than 1.5×10^{-4} Ω cm. There is also such a requirement that the films used for STN type color LCD must be deposited at the substrate temperature (T_s) lower than 200–250 °C and the resistivity must be lower than 2.0×10^{-4} Ω cm.[1] Several approaches to get the low resistivity films have been successfully made by reactive evaporation using tungsten electron emitters,[2,3] rf magnetron sputtering,[4] and dc magnetron sputtering.[5] The reasons for the low resistivity, however, have not been elucidated yet, probably because of the complex structure of the unit cell of crystalline In_2O_3 which consists of 80 atoms and the complex nature of the conducting mechanisms in polycrystalline films.

We already reported on the different dependences of electrical and structural properties on the thickness of the ITO films between different preparation methods, i.e., the conventional dc magnetron sputtering (SP) and electron beam evaporation (EB).[6] In this study the films with the reproducible resistivity less than 1.35×10^{-4} Ω cm were formed at $T_s = 350$–400 °C by applying highly dense plasma both to the dc magnetron sputtering and EB evaporation systems. The crystallinity and chemical states of the dopants of these films were investigated with relation to the electrical properties. The films were also deposited at the lower T_s of 60–280 °C and the drastic changes of the electrical and structural properties with the post-annealing were investigated, which were highly relevant to our interpretation of the high conductivity of the films.

II. EXPERIMENT

A. Preparation of the films

1. Low-voltage dc magnetron sputtering (LVMS)

Isibashi *et al.* reported that the resistivity of the ITO films deposited by dc magnetron sputtering had a clear positive relationship with sputtering voltages (V_{sp}).[5] It was also reported by Chang *et al.* that magnetic field strength at the cathode surface (MFS) dominates the current-voltage (I-V) characteristics and offsets threshold V_{sp} requirement in the dc planar magnetron sputtering system.[7]

In this study the V_{sp} was lowered from 540 to 330 V at the same sputtering current by increasing the MFS (Table I). Plasma diagnosis was carried out by plasma emission monitoring using the optical spectrum analyzer (GUIDED WAVE INC. MODEL-200) with the telescope in order to estimate plasma density and electron temperature near the surface of the target with high spatial resolution. The SnO_2 dopant content in the sintered oxide target was 10 wt% and the sputtering gas was a mixture of Ar and 0.8–1.0% O_2 at volume ratio, which were optimum values for the films with the lowest resistivity. Water partial pressure of the residual gas was controlled to be less than 10^{-5} Torr using a quadrupole mass spectrometer (ULVAC MSQ150A) in order to guarantee high reproducible film properties.[8] The ITO films with thickness of about 1200 Å deposited on SiO_2-coated soda lime glass substrates at 400 °C.

[a]Present address: Brown University, Division of Engineering, Box D, Providence, RI 02912.

 0021-8979/92/073356-09$04.00

TABLE I. The electrical and structural properties of the sputtering ITO films deposited at different V_{sp} ($T_s = 400$ °C).

Magnetic field: MFS (G)	Sputtering voltage: V_{sp} (V)	Sputtering current (A)	Thickness (Å)	Resistivity ($\times 10^{-4}$ Ω cm)	Carrier density ($\times 10^{20}$ cm^{-3})	Mobility (cm^2/V s)	Grain size[a] (Å) (222)	(400)	Uniform strain (%) (222)	(400)	Grain orientation[b] $I(400)/I(222)$	Sn 3d/In 3d Top surface	Inside	Surface/Inside
140	540	2.7	1140	1.92	7.48	43.0	256	264	1.39	1.23	2.02	0.175	0.097	1.80
350	380	2.7	1370	1.34	10.5	42.9	218	235	1.35	1.08	3.20	0.186	0.071	2.62
480	330	2.7	1240	1.35	10.3	43.1	215	239	1.41	1.07	3.80	0.209	0.075	2.79

[a]These values were calculated by the Scherrer method (see Ref. 10) using x-ray diffraction peak and were in the direction normal to the surface of the films.
[b]The value for the random orientation by ASTM is 0.33.

2. Highly dense plasma-assisted EB evaporation (HDPE)

Figure 1 illustrates the schematic drawing of the (HDPE) system.[9] The deposition chamber has a set of arc plasma generators and crucible containing sintered ITO pellets including 7.5 wt% of SnO_2 dopant. In arc plasma, the ionization ratio of gas is several tens percent and the densities of ions, electrons, and activated neutral particles are much higher than conventional dc or rf glow discharges. The chamber was filled with a mixture of Ar and 0–50% O_2 at volume ratio and the total gas pressure was $3–5 \times 10^{-4}$ Torr. The HDPE films were deposited at T_s of 60–350 °C on the same substrates as used in the low voltage magnetron sputtering (LVMS) films.

B. Characterization of the films

The resistivity, free-carrier density, and Hall mobility of the films were determined by the four-point probe method and Hall-effect measurement. The films thickness was measured using a Talystep apparatus. The x-ray diffraction was carried out with 50 kV, 120 mA Cu $K\alpha$ radiation (Rigaku, RU-200RAD-B) using a diffracted beam curved crystal monochromator (Rigaku, CN2726A1). The $K\alpha_1\alpha_2$ doublets in the diffraction peaks were separated by the Rachinger method[10] to get the pure line profile for $K\alpha_1$. Instrumental peak broadenings were calibrated by Si powder annealed at 900 °C. The uniform strains were determined from the center of gravity of the diffraction peaks and the random strains were determined by the integral breadth method.[10] Close analyses on surface morphology and substructures were carried out using FE-SEM and conventional TEM (Philips 420, 120 kV), respectively. Sn segregation at the surface was evaluated by ESCA.

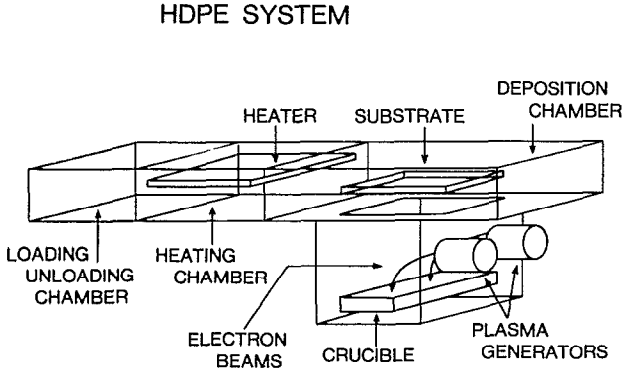

FIG. 1. Schematic illustration of the highly dense plasma-assisted EB evaporation (HDPE) system.

III. RESULTS AND DISCUSSION

A. LVMS films

In order to lower the plasma impedance and deposit the films at the lower V_{sp}, the stronger magnetic field was applied to the target for the conventional dc planar magnetron sputtering system. For an investigation on the effects of MFS on the plasma parameters the emission spectra from the plasma close to the surface of the target were measured for the MFS of 140, 350, and 480 G in the range

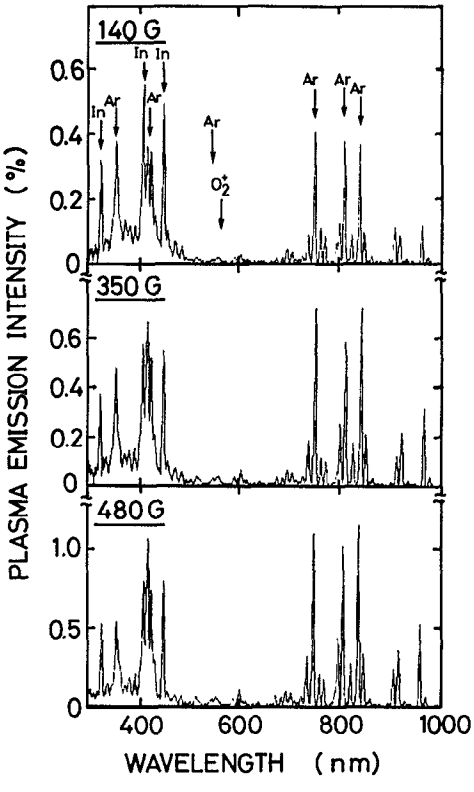

FIG. 2. Plasma emission spectra from the dc magnetron sputtering system at various magnetic field strength (MFS) at the cathode surface; 140, 350, and 480 G. The intensities of the emission spectra were calibrated using the standard halogen lamp.

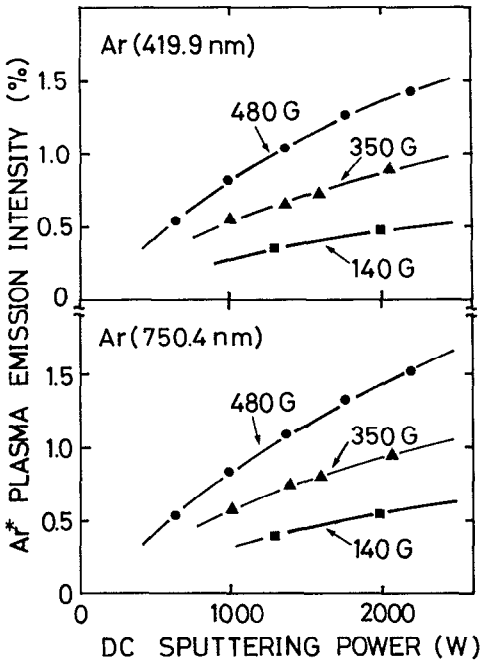

FIG. 3. Ar* plasma emission intensity from the dc magnetron sputtering system as a function of the sputtering power for the various MFS (■) 140 G, (▲) 350 G, and (●) 480 G.

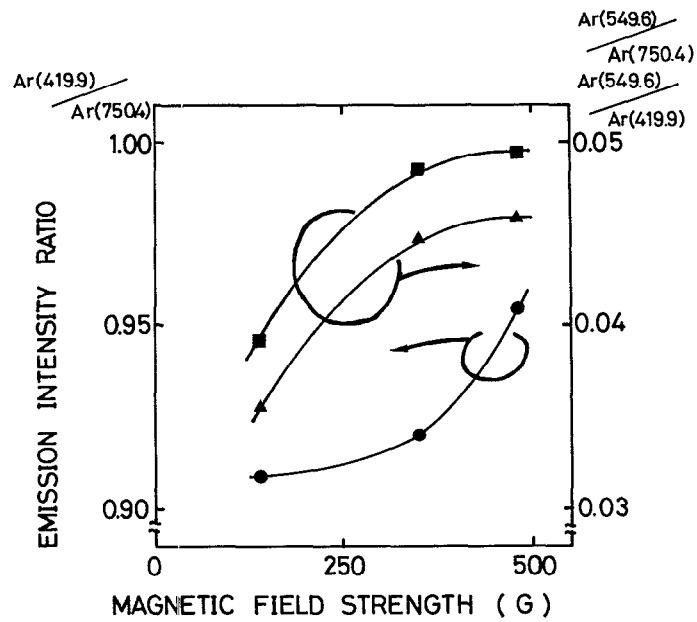

FIG. 4. Ar* emission intensity ratios as a function of the MFS (■) Ar(549.6)/Ar(419.9), (▲) Ar(549.6)/Ar(750.4), and (●) Ar(419.9)/Ar(750.4).

from 300 to 1000 nm (Fig. 2). All strong peaks were assigned to activated neutral radicals: Ar* and In*.[11–13] The Ar* plasma emission intensities for the different MFS are shown in Fig. 3 as a function of the dc sputtering power. The emission intensity, which corresponds to the plasma density,[14] increased more rapidly for the larger MFS as the power increased. The electron temperature, i.e., the electron mean energy in the plasma, was also estimated qualitatively by the Ar* emission intensity ratio between two different lines which had different excitation energies.[15] The excitation energies from the ground state (E_i) are shown in Table II for the lines of Ar(419.9), Ar(549.6), and Ar(750.4). The intensity ratios of (higher E_i)/(lower E_i): Ar(419.9)/Ar(750.4), Ar(549.6)/Ar(750.4), and Ar(549.6)/Ar(419.9) are shown in Fig. 4 as a function of the MFS at the same sputtering power of 1300 W. A certain increase in the electron temperature was observed with the increase in the MFS. In the magnetron systems the electron is trapped near the surface of the target and moves in the cycloidal orbit with the Larmor radius $r=m_e v/eB$, where B and v are the MFS and electron velocity, respectively.[16] As the density and staying time of the trapped electrons at the cathode sheath increased with the increase in B, the ionizing effect increased and the electrons can get more energy from the electric field, which might have increased the plasma density and the electron temperature near the surface of the target. As a result, the V_{sp} was lowered from 540 to 330 V at the same sputtering current of 2.7 A by increasing MFS from 140 to 480 G.

TABLE II. The excitation energies (E_i) of the Ar* plasma emission lines with the transition $i \rightarrow j$ (see Ref. 11).

Wavelength (nm)	E_i (eV)	E_j (eV)
419.9	$5p(2\frac{1}{2})$:14.50	$4s(1\frac{1}{2})°$:11.55
549.6	$6d(3\frac{1}{2})°$:15.33	$4p(2\frac{1}{2})$:13.08
750.4	$4p'(\frac{1}{2})$:13.48	$4s'(\frac{1}{2})°$:11.83

Table I shows the room-temperature resistivity (ρ), Hall mobility (μ), and free-carrier density (n) for the films deposited at the different V_{sp}. ρ decreased from 1.92 to 1.34×10^{-4} Ω cm with the decrease in the V_{sp} from 540 to 380 V due mostly to the increase in n. The SEM images of these films are shown in Fig. 5. All the images seem quite similar to each other, showing the typical morphology of the SP ITO films[6] with a grain size of 200–300 A and the flat surfaces with a comparison of the films prepared by EB evaporation. The ordinary x-ray diffraction patterns are shown in Fig. 6. The integrated intensity ratio of (400) peak to (222) peak [$I(400)/I(222)$] was 2.02 for the films deposited at $V_{sp}=540$ V, whereas the values for the random orientation by ASTM was 0.33, which indicated a preferred orientation of the grains in the ⟨100⟩ direction. With the decreasing V_{sp} the preference for the ⟨100⟩ direction became stronger, which was the same tendency as the predominant orientation with increasing T_s for the SP ITO films.[17]

To determine the lattice parameters and grain sizes in the direction normal to the film surface, the correct x-ray diffraction peak profiles were measured in the step scan mode with a step interval of 0.01° (Fig. 7). The grain size calculated by the Scherrer method[10] and the ratios of lattice parameters to those in ASTM (uniform strains) are shown in Table I. The grain sizes in the direction normal to

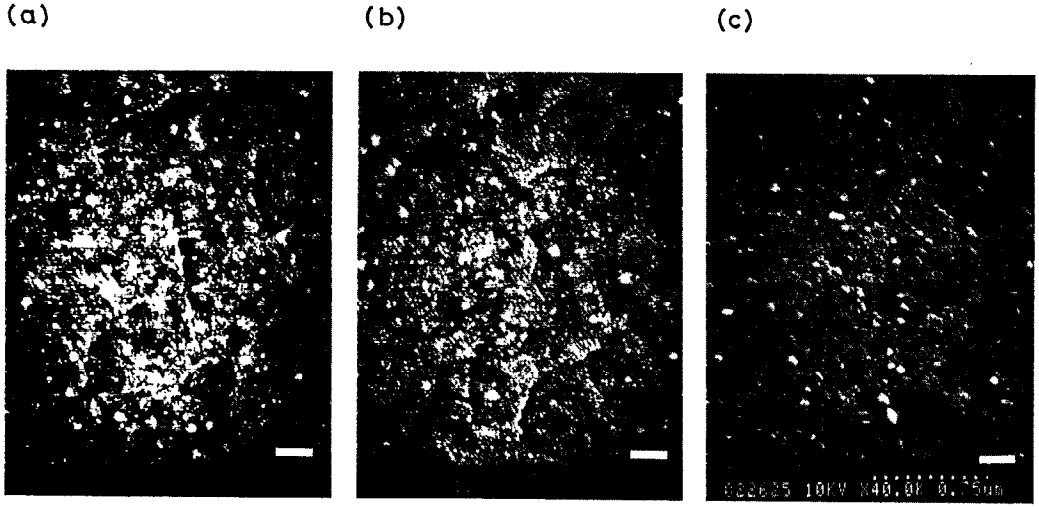

FIG. 5. SEM images of the ITO films with the thickness of about 1200 Å deposited by dc magnetron sputtering at the different V_{sp}: (a) 330 V, (b) 380 V, and (c) 540 V. Markers represent 2500 Å.

the surface of the films were 210–270 A, which were similar to the values in the direction parallel to the surface estimated by the SEM images. The slightly smaller sizes of the ⟨111⟩ orientated grains for lower V_{sp} films might be caused by the weaker orientation distribution in this direction. The uniform strain estimated by (400) peak, which was diffracted by the grains in the preferred ⟨100⟩ orientation, showed steady decrease from 12.3 to 1.08% with the decrease in V_{sp} from 540 to 380 V. As the increase in the lattice parameter reflects the crystallinity of the SP ITO films,[6] the decrease in the uniform strain indicates the increase of crystallinity.

Sn segregation at the grain boundaries has been shown to exist by SAM analysis on the fractured surface of the 1-μm-thick EB evaporated and ion-plated ITO films.[3] Their results of ESCA analysis on the top surface of the 1000 Å films were in good agreement with the view that Sn was segregated at grain boundaries. Therefore the top surface can also be considered to act like a boundary. Table I also shows peak intensity ratios of Sn 3d/In 3d at the top surface and inside the films, as measured by ESCA. As can be seen from the table, the segregated Sn atoms at the grain boundaries increased with the decreasing V_{sp}, which corresponded to the higher crystallinity of the LVMS films probably caused by the more calm crystal growth with less damages during the deposition.

It is well known for the ITO films that the donors are liberated from the substitutionally entered Sn atoms in the cation sublattice and from the doubly charged oxygen

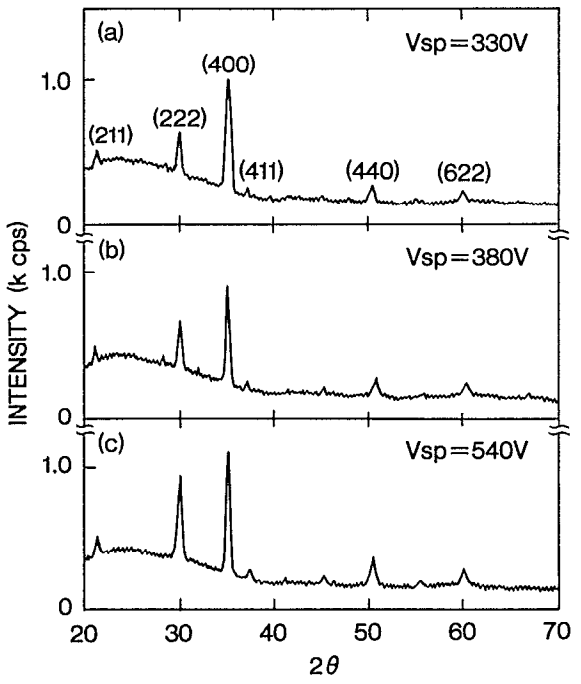

FIG. 6. X-ray diffraction patterns of the ITO films with the thickness of about 1200 Å deposited by dc magnetron sputtering at the different V_{sp}: (a) 330 V, (b) 380 V, (c) 540 V.

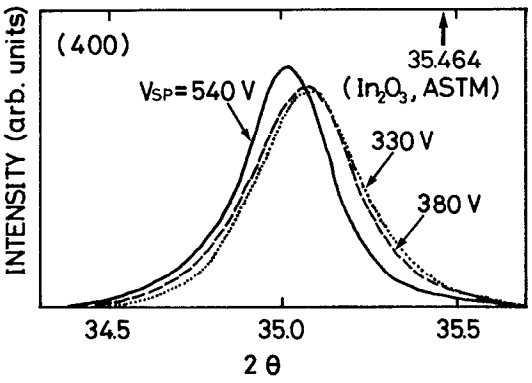

FIG. 7. (400) X-ray diffraction peaks of the ITO films deposited by dc magnetron sputtering at the different V_{sp}. The $K\alpha_1\alpha_2$ doublets were separated by the Rachinger method (see Ref. 10) and the pure line profiles for $K\alpha_1$ were shown.

TABLE III. The electrical and structural properties of the HDPE films deposited at 350 °C with the comparison of the films prepared by conventional EB evaporation and dc magnetron sputtering.

	Thickness (Å)	Resistivity ($\times 10^{-4}\Omega$ cm)	Carrier density ($\times 10^{20}$ cm^{-3})	Mobility (cm^2/V s)	Grain Size[a] TEM (Å)	Grain Size[b] x ray (Å)	Random strain (%)	Uniform strain (%) (222)	(440)	Sn 3*d*/In 3*d* Top surface	Inside	Surface/ Inside
HDPE	2130	1.35	13.3	34.8	500–700	525	0.15	1.04	0.68	0.115	0.090	1.28
EB[c]	1970	2.02	8.18	37.8	500–1500	963	0.16	0.43	0.39	0.120	0.041	2.93
SP	2160	1.63	9.28	41.0	350–500	414	0.26	0.99	0.88	0.183	0.091	2.01

[a]These values were estimated by conventional TEM analysis (Philips 420, 120 kV) and were in the direction parallel to the surface of the films.
[b]These values were calculated by the integral breadth method (see Ref. 10) using x-ray diffraction data and were in the direction normal to the surface of the films.
[c]Source material was sintered ITO pellet with 5.0 wt % SnO_2.

vacancies.[18] Since only 3.5 wt% SnO_2 is needed for a 1×10^{21} cm^{-3} carrier density, even if we assume that all the free electrons are provided by Sn atoms, more than 6.5 wt % SnO_2 must be electrically inactive in our sputtering films. This might be because of the lower crystallinity of the films caused by the bombardments of two kinds of high-energy particles already reported for the sputtering system, i.e., high energy neutrals (Ar) produced by neutralization of positive ions (Ar^+) at the surface of the target[19] and energetic negative ions (O^-).[20] As both of these particles were accelerated in the cathode sheath to the direction of the substrate, the films with higher crystallinity could be deposited at the lower V_{sp}. This higher crystallinity results in a decrease in concentration of dopants (Sn or oxygen vacancy) trapped at crystalline defects, and hence increase electrically active species inside each grain.

B. HDPE films (T_s=350 °C)

The electrical and structural properties of the HDPE films are shown in Table III with a comparison of the conventional EB and SP films deposited at the same T_s of 350 °C. With the assistance of the high dense plasma in the EB evaporation system, ρ of the HDPE films decreased from 2.02 to $1.35\times10^{-4}\,\Omega$ cm due mostly to increase in n. SEM image of these films is shown in Fig. 8. The HDPE film had a smoother surface than the EB film and a texture of the domains with an average diameter of 2000–3000 Å. Close analysis by conventional TEM revealed that each domain consisted of well-oriented subgrains of the order of 500–700 Å. Figure 9 shows ordinary x-ray diffraction patterns. Both the EB and HDPE films showed the strong (222) peaks, which indicated ⟨111⟩ preferred orientations, whereas the SP films showed strong ⟨100⟩ preferred orientation.

The correct x-ray diffraction peaks were also measured for these films to determine the extension of the lattice parameter (uniform strain), the random strain, and the grain size (Fig. 10). The uniform strain of the EB films determined by the shift of the strongest (222) peak increased from 0.43 to 1.04% by applying high density arc plasma (Table III). For the broadening of the x-ray diffraction peak, three origins are considerable: the instrumental factor, the small grain size, and the random strain. Several methods can be employed to separate these factors. In this study an integral breadth method was used.[10] The integral breadth β is defined as

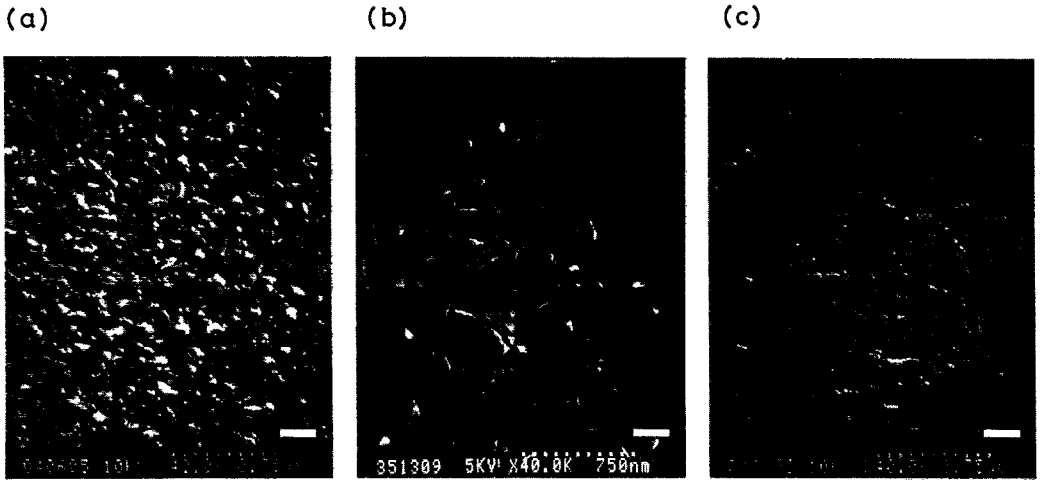

FIG. 8. SEM images of the ITO films with the thickness of about 2000 Å deposited by the different methods: (a) conventional EB, (b) HDPE, and (c) conventional SP (V_{sp} = 540 V). Markers represent 2500 Å.

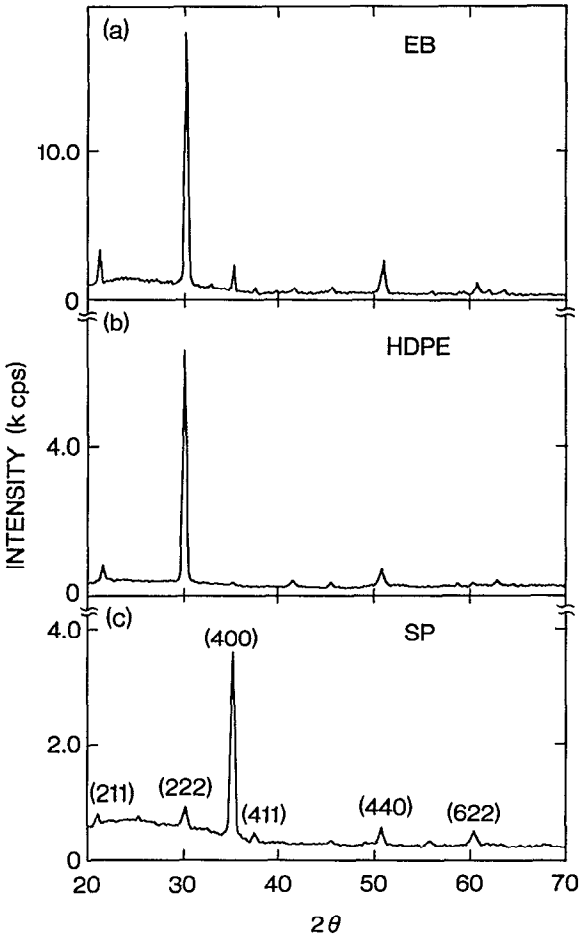

FIG. 9. X-ray diffraction patterns of the ITO films with the thickness of about 2000 Å deposited by the different methods: (a) conventional EB, (b) HDPE, and (c) conventional SP ($V_{sp} = 540$ V).

$$\beta = \int \frac{I(2\theta)d\theta}{I_{max}}, \tag{1}$$

where $I(\theta)$ is the diffracted intensity as a function of scattering angle 2θ. The diffraction peaks of these films were

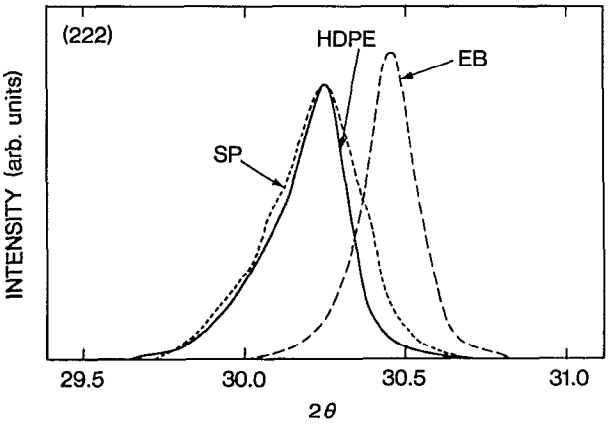

FIG. 10. (222) X-ray diffraction peaks of the ITO films deposited by the different methods: EB, HDPE, and SP. The pure line profiles for $K\alpha_1$ were determined using the Rachinger method (see Ref. 10).

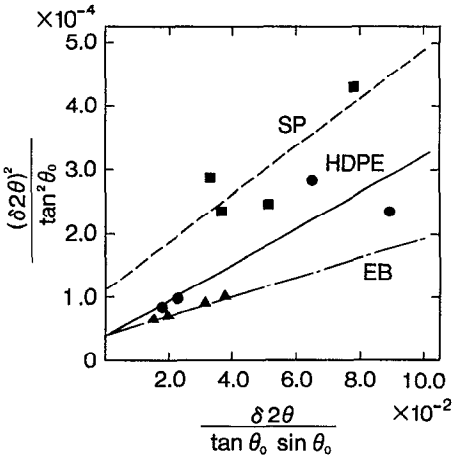

FIG. 11. Linear plot of $(\delta 2\theta)^2/\tan^2\theta_0$ against $\delta 2\theta/(\tan\theta_0 \sin\theta_0)$ for (222), (400), (440), and (622) peaks of the EB, HDPE, and SP films.

better fit with a Gaussian function rather than a Cauchy function, the true diffraction peak integral breadth β_t was calculated by

$$\beta_t^2 = \beta_b^2 - \beta_i^2, \tag{2}$$

β_b is the measured broadened peak integral breadth, and β_i is the instrumental peak broadening breadth determined by the diffraction peaks of Si powder annealed at 900 °C. Approximating the random strain broadening by a Gaussian function and the effect of small grain size by a Cauchy function, we obtain

$$\beta_s/\beta_t = 1 - (\beta_d/\beta_t)^2, \tag{3}$$

where β_s and β_d are the integral breadth due to small size and distortion, respectively.[21] The following approximate formula was used with the breadth in $\delta 2\theta$ (rad):

$$\frac{(\delta 2\theta)^2}{\tan^2\theta_0} = \frac{K\lambda}{L}\left(\frac{\delta 2\theta}{\tan\theta_0 \sin\theta_0}\right) + 16e^2, \tag{4}$$

where θ_0 is the positron of the peak maximum, λ is the wavelength of the x ray (Cu $K\alpha_1$), K is the Scherrer constant, L is the grain size, and e is an approximate upper limit on the lattice distortions.[10] The value of e corresponds to random strain. Linear plots of $(\delta 2\theta)^2/\tan^2\theta_0$ against $\delta 2\theta/(\tan\theta_0 \sin\theta_0)$ for (222), (400), (440), and (622) peaks are shown in Fig. 11 for the EB, HDPE, and SP films. As can be seen from Eq. (4), the grain size and random strain in a direction normal to the film surface could be determined from the slope $K\lambda/L$ and ordinate intercept $16e^2$ (Table III). The random strain of the HDPE films was 0.15%, which was the same level as the EB film and much smaller than the SP film. As the high dense plasma diffused closely to the substrate in the HDPE system, the substrate was bombarded by the large amount of Ar^+ with the energy of plasma potential: 10–15 eV. During the deposition this ion bombardment with much lower energy than in the SP system might result in a homogeneous strained structure with the narrow distributed large uniform strain, whereas in the SP system, the energy

TABLE IV. The electrical properties of the HDPE films deposited at 60–280 °C and post-annealed at 100–250 °C.

Substrate temperature (°C)	Annealing condition (°C)	Thickness (Å)	Resistivity ($\times 10^{-4}$ Ω cm)	Carrier density ($\times 10^{20}$ cm^{-3})	Mobility (cm^2/V s)
60	···	1860	4.92	4.19	30.3
60	100 °C, 20 min	1860	4.69	4.32	30.8
60	150 °C, 20 min	1870	4.51	4.73	29.3
60	200 °C, 20 min	1870	4.25	4.93	29.8
60	200 °C, 60 min	1890	3.64	6.44	26.7
145	···	2060	3.09	4.38	46.2
145	180 °C, 20 min	2060	2.76	6.59	34.3
145	250 °C, 20 min	2060	2.39	6.45	40.7
185	···	2050	1.77	14.0	25.3
185	180 °C, 20 min	2050	1.71	14.0	26.1
185	250 °C, 20 min	2050	1.67	13.4	28.0
280	···	3010	1.23	10.7	47.5
280	180 °C, 20 min	3010	1.23	10.6	47.7
280	250 °C, 20 min	3010	1.25	9.23	54.1

of the bombarding particles accelerated in the cathode sheath were a wide range of ~500 eV,[22] which might result in the inhomogeneity of the film crystallinity with both the large uniform strain and random strain.

The Sn segregation was also estimated for these three films by the same method as explained for LVMS films using ESCA (Table III). The HDPE film showed the much smaller Sn segregation than EB film. This might be caused by the activation of evaporated materials and the large amount of low-energy ion bombardment, which increased nucleation density and enhanced the chemical reaction at the surface of the film. The crystal growth process of the conventional EB deposition might be too moderate so that the impurity segregation takes place extremely. The higher carrier density for the HDPE films was thought to be the result of the effective Sn containment in each grain rather than the EB film and the homogeneous strained structure.

C. HDPE films (T_s=60–280 °C)

For further investigation on the relationship between the electrical properties and the structure, the HDPE ITO films with various levels of the crystallinity were deposited at T_s of 60–280 °C and the changes of these properties by post-annealing at T_a of 100–250 °C in the air were analyzed for each film. The results are listed in Table IV. The crystallization temperature for the amorphous ITO films was reported to be about 150 °C.[23] The changes of the electrical properties by post-annealing at the different T_a are shown in Fig. 12 for the films deposited at 60 °C, which were confirmed to be amorphous before the post-annealing by x-ray diffraction. The ρ decreased by post-annealing due to the increase in n in spite of some decrease in μ, and these changes were more remarkable at a higher T_a of 200 °C. For the films deposited at T_s of 145 °C the changes in the electrical properties showed the same tendency, i.e., decrease in ρ, μ, and increase in n. Whereas the films deposited at T_s of 185 and 280 °C showed quite different changes in the electrical properties, i.e., the slight decrease in ρ due to the increase in μ in spite of the slight decrease in n. The SEM images of the films as deposited at T_s = 145, 185 °C and the film of T_s = 145 °C post-annealed at 180 °C for 20 min are shown in Fig. 13. The films as-deposited at T_s = 145 °C showed a quite flat surface with no textures and after post-annealing a texture of the domains with a

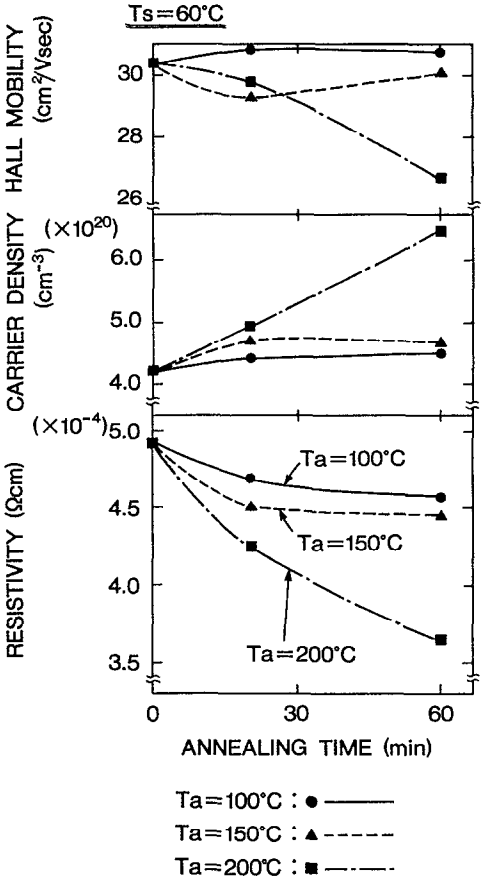

FIG. 12. Electrical properties of the HDPE ITO films deposited at T_s = 60 °C as a function of the post-annealing time at the various post-annealing temperatures: T_a = 100, 150, and 200 °C.

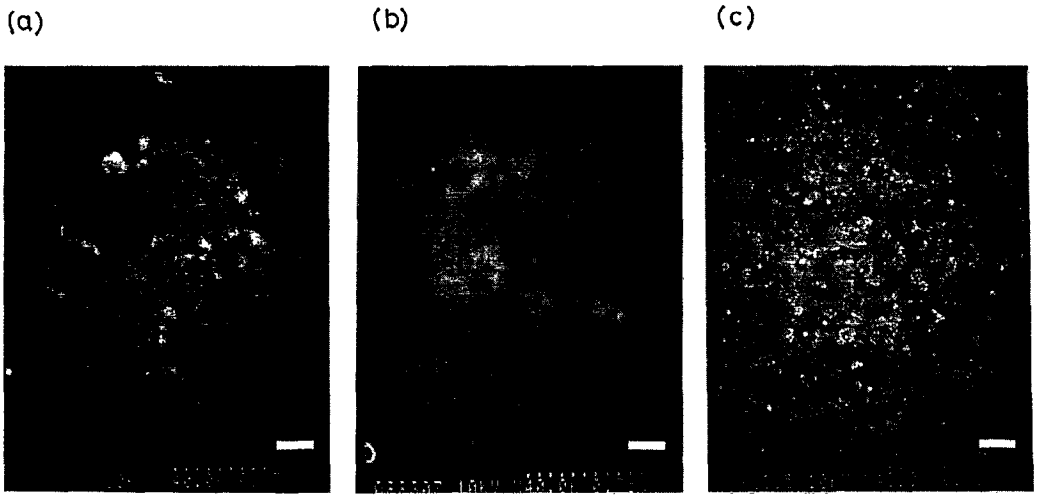

FIG. 13. SEM images of the HDPE ITO films of the different T_s and T_a: (a) as-deposited at $T_s = 145$ °C, (b) $T_s = 145$ °C and post-annealed at $T_a = 180$ °C for 20 min, and (c) as-deposited at $T_s = 185$ °C. Markers represent 2500 Å.

diameter of 1000–3000 Å was observed, whereas the film as-deposited at $T_s = 185$ °C showed the texture of the domains with a diameter of about 1000–1500 Å consisted of the subgrains with a diameter of about 200 Å. X-ray diffraction patterns for these films are shown in Fig. 14. The film as-deposited at $T_s = 145$ °C showed a mixture of the amorphous and crystalline structures, and crystallization of the amorphous phase occurred completely by post-annealing at 180 °C for 20 min. The film as-deposited at $T_s = 185$ °C showed crystalline structure and did not change with postannealing at 250 °C. From this evidence that the large increase in n with the post-annealing for the films deposited at lower T_s than 145 °C must be caused by the drastic improvement in crystallinity and the increase in the electrically active species, which were already discussed for the LVMS films. The decrease in μ with the post-annealing can be explained by the segregation of Sn, the increase in ionized impurity density,[24] and the formation of the grain boundaries caused by the crystallization. Whereas the as-deposited films at higher T_s than 185 °C had complete crystalline structure, so the decrease in n with the post-annealing might be caused by the oxidation of the films and the extinction of some amounts of oxygen vacancies.

IV. CONCLUSIONS

The ITO films with the reproducible resistivity less than 1.35×10^{-4} Ω cm were deposited by applying the highly dense plasma both to the dc magnetron sputtering and EB evaporation. The detailed structural analyses using x-ray diffraction, ESCA, and SEM revealed that the conventional SP film showed low crystallinity with many crystallographic faults caused by the bombardment of the high

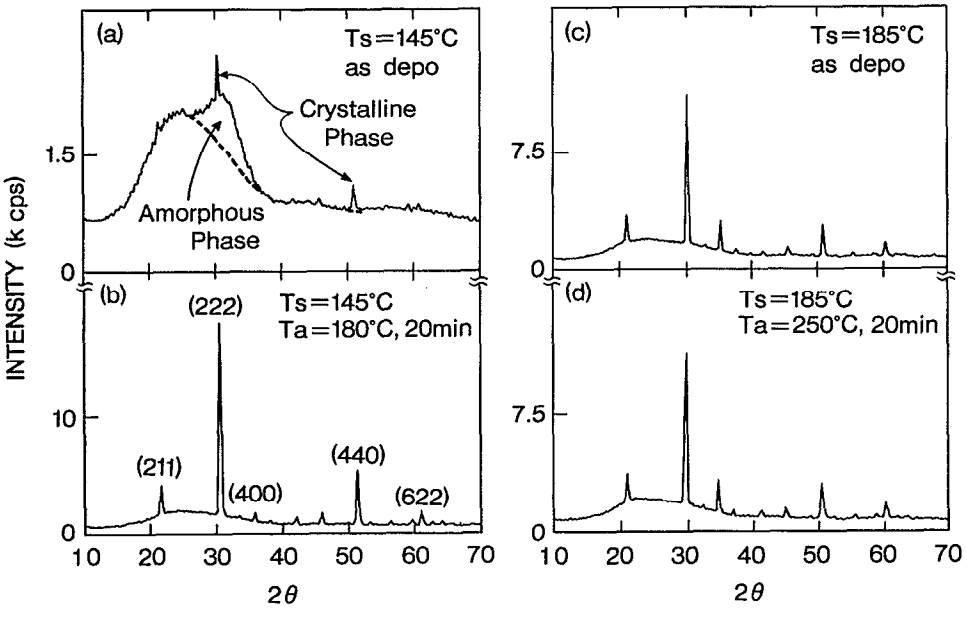

FIG. 14. X-ray diffraction patterns of the HDPE ITO films of the different T_s and T_a: (a) as-deposited at $T_s = 145$ °C, (b) $T_s = 145$ °C, and post-annealed at 180 °C for 20 min, (c) as-deposited at 185 °C, and (d) $T_s = 185$ °C and post-annealed at 250 °C for 20 min.

energy particles during deposition, which might increase the electrically inactive dopants trapped at the structural defects. By applying the stronger magnetic field to the SP system, plasma impedance was decreased and lower damaged films were deposited, which showed the low resistivity of 1.34×10^{-4} Ω cm. Whereas the conventional EB films consisted of the large size grains with good crystallinity, a large amount of Sn segregated at the surface and the grain boundaries. By applying the arc plasma to the EB system, the chemical reaction at the surface of the film was enhanced and the Sn segregation decreased. The film with resistivity of 1.23×10^{-4} Ω cm was deposited at T_s of 280 °C by this HDPE system. The effect of the crystallinity on the electrical properties was confirmed by the analyses on the films deposited at T_s of 60–280 °C and their post-annealing.

ACKNOWLEDGMENTS

The authors are grateful to Professor D. C. Paine of Brown University for a critical reading of the manuscript. They also thank Dr. K. Suzuki and T. Oyama for making valuable suggestions, and Y. Hayashi and the Material Analysis Group in Asahi Glass Co., Ltd. for the ESCA and SEM analyses.

[1] H. Koh, K. Sawada, M. Ohgawara, T. Kuwata, H. Tubota, M. Akatsuka, and M. Matsuhiro, SID Dig. Tech. Papers, 53 (1988).
[2] P. Nath, R. F. Bunshah, B. M. Masel, and O. M. Stuffsud, Thin Solid Films **72**, 463 (1980).
[3] S. Takaki, K. Matsumoto, and K. Suzuki, Appl. Surf. Sci. **33/34**, 919 (1988).
[4] S. Ray, R. Banerjee, N. Basu, A. K. Batabyal, and A. K. Barna, J. Appl. Phys. **54**, 3497 (1983).
[5] S. Ishibashi, Y. Higuchi, Y. Ota, and K. Nakamura, J. Vac. Sci. Technol. A **8**, 1403 (1990).
[6] Y. Shigesato, S. Takaki, and T. Haranoh, Appl. Surf. Sci. **48/49**, 269 (1991).
[7] S. A. Chang, M. B. Skolnik, and C. Altman, J. Vac. Sci. Technol. A **4**, 413 (1986).
[8] Y. Shigesato, Y. Hayashi, A. Masui, and T. Haranoh, Jpn. J. Appl. Phys. **30**, 814 (1991).
[9] S. Takaki, Y. Shigesato, H. Harada, H. Kojima, T. Oyama, and T. Haranoh, SID Dig. Tech. Papers **21**, 76 (1990).
[10] H. P. Klug and L. E. Alexander, *X-Ray Diffraction Procedures for Polycrystalline and Amorphous Materials*, 2nd ed. (Wiley, New York, 1974), Chap. 9.
[11] A. R. Striganov and N. S. Sventitskii, *Tables of Spectral Lines of Neutral and Ionized Atoms* (IFI/Plenum Data, New York, 1968).
[12] J. Reader and C. H. Corliss, *Wavelengths and Transition Probabilities for Atoms and Atomic Ions*, Wavelength Tables, 4th printing (M.I.T., Cambridge, 1985), NSRDS-NBS, 1980.
[13] R. W. B. Pearse and A. G. Gaydon, *The Identification of Molecular Spectra* (Chapman and Hall, London, 1941).
[14] J. G. Cook and S. R. Das, J. Appl. Phys. **65**, 1846 (1989).
[15] H. Kawata, T. Nagaoka, and K. Murata, Proc. 7th Symp. on Plasma Processing, Tokyo, 1990, p. 149.
[16] B. N. Chapman, *Glow Discharge Processes* (Wiley, New York, 1980), Chap. 6.
[17] R. Latz, K. Michael, and M. Scherrer, Jpn. J. Appl. Phys. **30**, 2A, L. 149 (1991).
[18] I. Hamberg, Ph. D. thesis, Chalmers University of Technology, Gothenburg, Sweden, 1984.
[19] I. Brodie, L. T. Lamont, Jr., and R. J. Jepsen, Phys. Rev. Lett. **21**, 1224 (1968).
[20] K. Tominaga, T. Yuasa, M. Kume, and O. Tada, Jpn. J. Appl. Phys. **24**, 944 (1985).
[21] M. Tromel and H. Hinkel, Ber. Bunsenges. Phys. Chem. **69**, 725 (1965).
[22] K. Tominaga, S. Iwamura, Y. Shintani, and O. Tada, Jpn. J. Phys. **21**, 688 (1982).
[23] S. Muranaka, Y. Bando, and T. Takeda, Thin Solid Films **151**, 335 (1987).
[24] G. Frank and H. Kostlin, Appl. Phys. A **27**, 197 (1982).